Stokes Flow in Channel Geometry as a Linear System of Equations on a Directed Graph

Haiyang Wang, Nils Jan Fredrik Fryklund, Samuel Potter, Leslie Greengard

November 22, 2022

Abstract

In this paper, we exploit the *return to Poiseuille* phenomenon: a Stokes flow would quickly develop to the Poiseuille flow along a straight channel. This allows us to quickly solve the interior plane Stokes equation on a domain that is a union of *standard pieces*. Each standard piece is a pipe with inlets/outlets being long enough straight channels, such that when two standard pieces are connecting, where they connect is in middle of a long straight channel*, hence the flow at the connection would be close to Poiseuille flow within machine precision. Then, instead of solving stokes equation for the global domain, we can solve the Stokes equation for each standard pieces with boundary condition of Poiseuille velocity profile at inlets/outlets, and easily interface these local solutions to build a solution for the global domain.

Once the Stokes equation with boundary conditions of Poiseuille velocity profile is pre-solved on each standard piece, the standard pieces can be connected to form a complex domain of channel network. Interfacing the solutions of standard pieces would instantly give a high-order accurate solution of Stokes equation for the global domain. For example, in Figure 1, interfacing the local solutions took only 0.3 seconds, while directly solving on the global domain took 24 minutes.

1 Introduction

The *return to Poiseuille* phenomenon, or *Saint-Venant's principle* in the theory of plane elasticity, are well-established from the last century [2, 6, 8]. To be more specific, in a straight channel with laminar and incompressible incoming flow, the flow would quickly converge into a Poiseuille flow: the difference of the flow and the Poiseuille flow would decay at an exponential rate for Stokes flow. Therefore it is a good numerical hypothesis to assume that a Stokes flow is Poiseuille in middle of a lone straight channel, regardless of the incoming and outgoing flow.

For plane Stokes flow, the biharmonic equation formulation have been developed within the theory of complex variable from the last century [9]. Various numerical methods, such as boundary integral equation (BIE) and rational function approximation, have been developed accordingly [5, 13]. The biharmonic BIE is adopted in this paper to solve the Stokes equation [5].

The main idea of this paper is to apply *Return to Poiseuille* as a high order accurate numerical hypothesis. It allows us to pre-solve several standard pieces which are pipes with inlets and outlets being long enough straight channels, and are with boundary condition of Poiseuille velocity profile. Once the standard pieces pre-solved, the *Return to Poiseuille* hypothesis allows us to interface solutions of Stokes flow on each standard pieces to get a solution for any complex channel geometry that is a union of the standard pieces. Interfacing is by solving a system of linear equations, based on the constraints of zero-net-flux and continuity of pressure. This system of linear equations can be solved instantly and accurately.

This paper is organized as follows. In Section 2, we define the Stokes boundary value problem (BVP), the corresponding biharmonic BVP, and then the BIE of it. We also mention the analytic evidence and predicted exponential convergence rate for the *return to Poiseuille* hypothesis. Then, we explain how to interface the local solutions of standard pieces by a simple example. In Section 3, we presents the Nyström discretization of the integral equation, which is solved iteratively by Generalized Minimal Residual Method (GMRES). The numerical experiments of connecting standard pieces and numerical evidence for *return to Poiseuille* hypothesis are contained in Section 4, followed by conclusions and possible further work in Section 5.

2 Mathematical Preliminaries

In this section, we briefly review the plane Stokes equation, its biharmonic formulation, and the BIE. More detailed discussion can be found in [5]. Then, we will present an analytic estimate for the exponential decay rate of *return to Poiseuille* hypothesis [6], and explain how we have applied it as a numerical hypothesis: how to pre-solve each standard pieces and how to interface the pre-solved solutions for a domain of connected standard pieces.

*The length of straight channel is greater than 7 times of the width, as indicated by Figure 5.

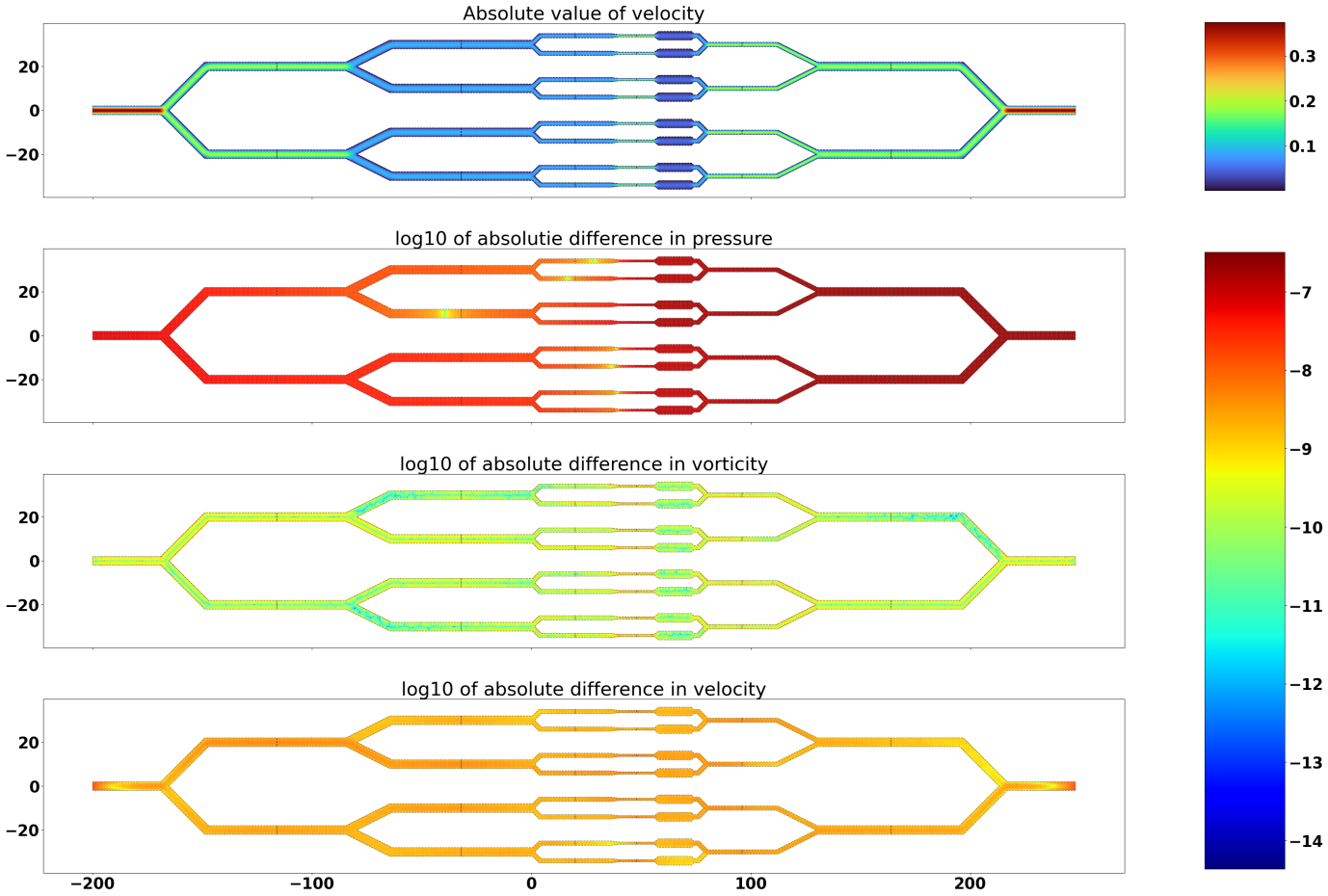

Figure 1: Solutions of the Stokes equation in a complex channel geometry as a union of 22 pieces of 7 different standard pieces. The first sub-figure is a color-plot of magnitude of velocity field inside the domain, with colorbar on its right. The black lines in the first sub-figure marks the boundary of each standard piece. The other three sub-figures are color-plots of absolute differences between the interfaced solutions and the global solution in pressure, vorticity, and velocity field, in the $\log_{10}$ scale, with colorbar on on their right. Each standard pieces are solved with required accuracy of 10^{-12} and the global domain is solved with required accuracy of 10^{-10}.

2.1 Boundary Integral Equation

Stokes Boundary Value Problem. Recall that the plane Stokes equation is [9]:

$$\nu\Delta u = \frac{1}{\rho}\frac{\partial p}{\partial x}, \quad \nu\Delta v = \frac{1}{\rho}\frac{\partial p}{\partial y} \tag{1}$$

$$\frac{\partial u}{\partial x} + \frac{\partial v}{\partial y} = 0 \tag{2}$$

where u, v are components of velocity, p is the pressure, ρ and ν are the density and viscosity. Another physics quantity, the vorticity, is defined as:

$$\zeta = u_y - v_x \tag{3}$$

We are interested in interior BVP of Stokes equation on a bounded $(M+1)$-ply connected domain $D \subset \mathbb{R}^2$, with boundary $\partial D = \Gamma = \Gamma_0 \cup \Gamma_1 \cup \cdots \cup \Gamma_M$, where Γ_0 is the exterior boundary, and $\Gamma_1, \ldots, \Gamma_M$ are the interior boundaries. This paper concerns with Stokes equation with boundary condition of velocity u, v on the boundary Γ, for given functions h_1, h_2:

$$u(t) = h_2(t), \quad v(t) = -h_1(t), \quad t \in \Gamma \tag{4}$$

Biharmonic Equation. (2) implies the existence of the stream function $W(x, y)$ such that [5]:

$$\frac{\partial W}{\partial x} = -v, \quad \frac{\partial W}{\partial y} = u \tag{5}$$

Following (1) and (2), it is easy to see that the stream function satisfies the biharmonic equation (6), and the Dirichlet BVP (4) can be rewritten as the following biharmonic BVP [5]:

$$\Delta^2 W(x, y) = \Delta\zeta = 0, \qquad (x, y) \in D \tag{6}$$

$$\frac{\partial W}{\partial x} = h_1(t), \quad \frac{\partial W}{\partial y} = h_2(t), \qquad t \in \Gamma \tag{7}$$

Goursat's Formula. By the Goursat's formula, any plane biharmonic function $W(x, y)$ can be expressed in the

following form [11]:

$$W(x,y) = \mathrm{Re}(\bar{z}\phi(z) + \chi(z)) \tag{8}$$

where the Goursat's functions ϕ, χ are analytic functions of complex variable $z = x + yi$. In the following, we will be identifying $(x, y) \in \mathbb{R}^2$ with $z = x + yi \in \mathbb{C}$.

Velocity, pressure, and vorticity can be conveniently expressed with the Goursat's functions. The Muskhelishvili's formula (9) expresses velocity field and another formula (10) expresses the pressure and vorticity [11]:

$$-v + ui = \frac{\partial W}{\partial x} + i\frac{\partial W}{\partial y} = \phi(z) + z\overline{\phi'(z)} + \overline{\psi(z)} \tag{9}$$

$$\zeta + \frac{i}{\nu}p = 4\phi'(z) \tag{10}$$

where $\psi = \chi'$.

The biharmonic boundary value problem (6) and (7), using the Muskhelishvili's formula (9), can be rewritten as

$$\phi(t) + t\overline{\phi'(t)} + \overline{\psi(t)} = h(t), \quad t \in \Gamma \tag{11}$$

where $h(t) = h_1(t) + ih_2(t)$, and t is understood as a complex variable.

Sherman-Lauricella Representation. The Sherman-Lauricella representation of Stokes problem is a specific form of the Goursat's functions [5], which can be applied as an ansatz for BIE of the biharmonic BVP (11). It is formulated as follows:

$$\phi(z) = \frac{1}{2\pi i}\int_\Gamma \frac{\omega(\xi)}{\xi - z}d\xi + \sum_{k=1}^{M} C_k \log(z - z_k) \tag{12}$$

$$\begin{aligned}\psi(z) = {} & \frac{1}{2\pi i}\int_\Gamma \frac{\overline{\omega(\xi)}d\xi + \omega(\xi)\overline{d\xi}}{\xi - z} \\ & - \frac{1}{2\pi i}\int_\Gamma \frac{\overline{\xi}\omega(\xi)}{(\xi - z)^2}d\xi \\ & + \sum_{k=1}^{M}\left(\frac{b_k}{z - z_k} + \overline{C}_k \log(z - z_k) - C_k\frac{\overline{z}_k}{z - z_k}\right)\end{aligned} \tag{13}$$

where ω is an unknown complex density on Γ, z_k are arbitrary prescribed point inside the component curves Γ_k, and C_k, b_k are constants defined by:

$$C_k = \int_{\Gamma_k}\omega(\xi)|d\xi|, \quad b_k = 2\,\mathrm{Im}\int_{\Gamma_k}\overline{\omega(\xi)}d\xi \tag{14}$$

It is worth-noting that although ψ, ϕ might be multiple-valued, the velocity, pressure, and vorticity are single-valued functions of z.

Boundary Integral Equation. Plugging the Sherman-Lauricella representation (12) and (14) into equation (11), and letting a point z in the interior of D approach to a point on the boundary $t \in \Gamma$ in (11), the classical formulae for the limiting values of Cauchy-type integral gives us the following boundary integral equation for ω [10, 5]:

$$\begin{aligned}\omega(t) + {} & \frac{1}{2\pi i}\int_\Gamma \omega(\xi)d\ln\frac{\xi - t}{\overline{\xi - t}} - \frac{1}{2\pi i}\int_\Gamma \overline{\omega(\xi)}d\frac{\xi - t}{\overline{\xi - t}} \\ & + \sum_{k=1}^{M}\left(\frac{\bar{b}_k}{\overline{t - z_k}} + 2C_k\log|t - z_k| + \overline{C_k}\frac{t - z_k}{\overline{t - z_k}}\right) \\ & + \frac{\bar{b}_0}{\overline{t - z^*}} \\ & = h(t), \qquad\qquad t \in \Gamma\end{aligned} \tag{15}$$

The extra term $\frac{\bar{b}_0}{\overline{t-z^*}}$ vanishes when the zero-net-flux condition $\mathrm{Re}\int_\Gamma \bar{h}(t)dt = 0$ is satisfied, hence is omitted in the Nyström discretization of (15). The invertibility of this integral equation is similar to the standard proof of invertibility for elasticity problems [11, 5], and are omitted.

2.2 Return to Poiseuille

In this section, we will first show the analytic estimate for the *return to Poiseuille* phenomenon, which is based on eigenfunction analysis on a domain of a semi-infinite straight channel from the theory of plane elasticity [6]. Then, we explain how to apply the *return to Poiseuille* hypothesis, how to build local solutions of each standard pieces, and how to interface the solutions on standard pieces.

Analytic Estimate for Return to Poiseuille. On the domain of a semi-infinite straight channel $D_L = \{(x, y) \mid x \geq 0, |y| \leq L\}$, with the boundaries

$$\begin{aligned}\Gamma_L &= \Gamma_L^1 \cup \Gamma_L^2 \cup \Gamma_L^3 \\ &= \{(0, y)||y| \leq L\} \cup \{(x, L)|x \geq 0\} \cup \{(x, -L) \mid x \geq 0\}\end{aligned} \tag{16}$$

where Γ_L^2, Γ_L^3 are walls with the non-slippery boundary conditions, and Γ_L^1 is the inlet with boundary condition of an incoming laminar flow. *Return to Poiseuille* means that regardless of the boundary velocity profile on Γ_L^1, the flow's profile at $x = l$ will converge to Poiseuille flow of same flux as $l \to \infty$.

Without lost of generality, assume there is zero net flux across Γ_L^1. Then, *return to Poiseuille* is equivalent to return to the zero flow, i.e. the flows velocity profile at the vertical cross-section $x = l$ would converge to zero as $l \to \infty$. The BVP of this problem can be formulated as the following:

$$\frac{\partial W(x,y)}{\partial y} = W(x,y) = 0, \qquad (x,y) \in \Gamma_L^2 \cup \Gamma_L^3 \tag{17}$$

$$\frac{\partial W(0,y)}{\partial x} = f(y), \qquad (0,y) \in \Gamma_L^1 \tag{18}$$

$$\frac{\partial W(0,y)}{\partial y} = g(y), \qquad (0,y) \in \Gamma_L^1$$

where f, g are continuous and satisfy $f(\pm L) = g(\pm L) = \int_{-L}^{L} g(y)dy = 0$, for requiring the zero-net-flux and a continuity of boundary condition.

This biharmonic BVP is identical to the self-equilibrated traction BVP on a semi-infinite strip in the theory of elasticity studied [6, 8, 2]. According to their result, when f''', g''' exist and are of bounded variation, this problem has a unique solution spanned by the Papkovich-Fadle eigenfunctions [6]. The absolute value of first eigenfunction is dominated by:

$$e^{-xk/2L}, \quad k \simeq 4.2^{\dagger}$$

This gives the decay rate of *return to Poiseuille hypothesis*, which agrees with our numerical experiment in Figure 5.

Return to Poiseuille as a Numerical Hypothesis. Given the analytic estimate above, it is easy to see that in a straight channel with length greater than 8 times of the channel width, we can expect the flow to be Poiseuille with 14th digits of accuracy at the outlet regardless of the velocity profile on the inlet. Therefore, it is appropriate to require the inlets/outlets of the standard pieces to be such straight channels, and assign the Poiseuille boundary conditions on the inlets/outlets.

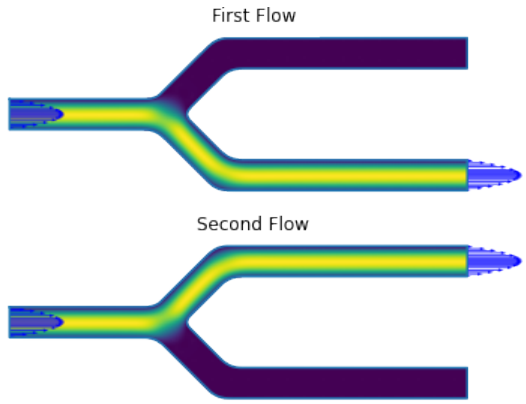

Figure 2: The 2 generating flows for a Y-shaped standard piece: the color inside the domain denotes the magnitude of the velocity of the flow, the blue arrow denotes the boundary condition of unit-flux Poiseuille velocity profile at the inlets/outlets.

Interface the Solutions on Standard Pieces. For a standard piece with a total number of m inlets/outlets, the boundary conditions of our interest, Poiseuille at the inlets/outlets and non-slippery elsewhere, can be simply characterized by the flux of the Poiseuille flow at each inlet/outlet. The fluxes need to sum to zero, so the boundary conditions is a $m-1$ dimensional space. As the Stokes equation is linear, this means we only need to solve for $m-1$ flows on the standard piece, and superimpose these flows would give us any flow in the standard piece with boundary condition of Poiseuille at inlets/outlet and non-slippery elsewhere. These flows are called *generating flows* in this paper. In practice, for a standard piece, we pick one of its inlets/outlets as the inlet for all generating flows, each of which would have one of the other inlets/outlets as an outlet. Figure 2 shows a standard piece of Y-shaped standard pieces, with a total number of 3 inlets/outlets, and are pre-solved with 2 generating flows of unit flux.

With the the generating flows pre-solved for each standard piece, interfacing these flows is reduced to finding appropriate fluxes of the generating flows of the standard pieces such that:

1. The fluxes matches at the interface of connection.
2. The pressure is a continuous function across the global domain.

The second condition is needed only when the global domain is not simply connected.

To demonstrate how these two conditions are turned into a linear system of equations for interfacing local solutions, let us consider the specific example in Figure 3a, where the global domain is two connected Y-shaped standard pieces. The global domain is given with flux $f_{-1} = 1$ (incoming) at the left inlet and flux $f_{-2} = 1$ (outgoing) at the right outlet. Each standard piece has two fluxes of generating flows need to be solved for, so there are total number of 4 fluxes f_0, f_1, f_2, f_3 needs to be solved for.

This problem can be abstracted into a problem of finding weights on edges of a directed graph as in Figure 3b, where the the nodes V_0, V_1, V_2, V_3 denotes the interfaces among the standard pieces and global boundary conditions of fluxes, The edge $E_{0,1}, E_{0,2}, E_{31}, E_{32}$ represents the generating flows with the fluxes f_0, f_1, f_2, f_3 to be solved for. The fluxes f_{-1}, f_{-2} are given on superficial edges representing the boundary fluxes of the global domain.

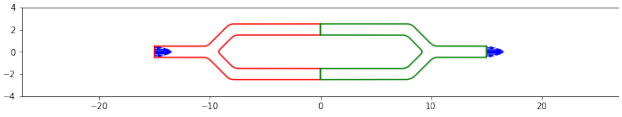

(a) The interface problem

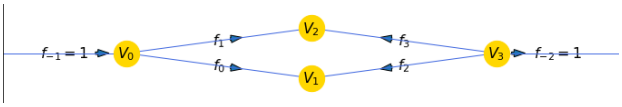

(b) The directed graph for the interface problem

Figure 3: A simple interface problem with 2 Y-shaped standard pieces.

The interface condition 1 of agreeing fluxes at the interfaces, in the directed graph, can be understood as the following: at each node, the incoming fluxes should be equal to outgoing fluxes. Requiring this to be true at all nodes gives us the following linear system of equations:

$$\begin{pmatrix} 1 & 1 & 0 & 0 \\ 1 & 0 & 1 & 0 \\ 0 & 1 & 0 & 1 \\ 0 & 0 & 1 & 1 \end{pmatrix} \begin{pmatrix} f_0 \\ f_1 \\ f_2 \\ f_3 \end{pmatrix} = \begin{pmatrix} f_{-1} \\ 0 \\ 0 \\ -f_{-2} \end{pmatrix} = \begin{pmatrix} 1 \\ 0 \\ 0 \\ -1 \end{pmatrix} \tag{19}$$

$^{\dagger}k$ is the smallest positive real parts of the roots of the transcendental equation $\sin^2 \lambda - \lambda^2 = 0$.

This matrix has rank 1 deficiency. This is due to the 1 cycle in the graph, and can be resolved by adding the continuity of pressure condition 2.

Continuity of pressure, or single-valued-ness of pressure, can be interpreted as that the pressure p_i at each node V_i is a well-defined single-valued function. And on a cycle, this means that the pressure drops along the cycle would sum to zero. Therefore, we can gain a new equation:

$$p_{10} + p_{31} + p_{23} + p_{02} = 0 \tag{20}$$

where p_{ij} is the pressure drop from node V_j to node V_i. The pressure drops p_{ij} depends linearly on the fluxes of generating flows of the standard pieces, For this case, p_{10}, p_{02} are linear functions of f_0, f_1, and p_{31}, p_{23} are linear functions of f_2, f_3. These linear functions can be computed in the pre-solving process, and for this example, they are

$$\begin{pmatrix} p_{10} \\ p_{02} \end{pmatrix} = \begin{pmatrix} 46.02 & 14.78 \\ -14.78 & -46.02 \end{pmatrix} \begin{pmatrix} f_0 \\ f_1 \end{pmatrix} \tag{21}$$

$$\begin{pmatrix} p_{31} \\ p_{23} \end{pmatrix} = \begin{pmatrix} -46.02 & -14.78 \\ 14.78 & 46.02 \end{pmatrix} \begin{pmatrix} f_2 \\ f_3 \end{pmatrix} \tag{22}$$

Combining equations (20), (21) and (22), we have:

$$(46.02 - 14.78)(f_0 - f_1 - f_2 + f_3) = 0 \tag{23}$$

which completes (19) to a full rank linear system of equations and with the solutions $(f_0, f_1, f_2, f_3) = (0.5, 0.5, -0.5, -0.5)$.

The process of interfacing local solutions in the example of Figure 3 can be generalized into a algorithm for interfacing of any connected standard pieces. The key idea of the algorithm is rather simple: generating the appropriate linear equations of matching fluxes and matching pressure drops, and then solving for fluxes of generating flows. However, it involves troublesome bookkeeping of the correspondence between the directed graph and the generating fluxes and pressure-drops of each standard pieces, so the complete description of the algorithm is omitted. [‡]

3 Description of Numerical Methods

In this section, we will first present Nyström discretization of BIE (15). And we will briefly mention several other numerical techniques we have adopted that are established for solving such BIE.

3.1 Boundary Integral Equation

The boundary curve Γ_k is given by the parametrization $\Gamma_k = \{t^k(a) : a \in [A_k, A_{k+1}]\}$, and discretized into N_k points $t_i^k = t^k(a_i^k)$. The exterior boundary Γ_0 is parameterized in the counter-clockwise orientation, while the interior boundaries are parameterized in the clockwise orientation. Associate to each point t_j^k are the unknown complex density ω_j^k, the derivative $d_j^k = t^{k\prime}(a_j^k)$, and the quadrature weight w_j^k. In total, we have $N = \sum_{k=0}^{M} N_k$ points. The Nyström discretization of BIE (15) is:

$$\omega_j^k + \sum_{m=0}^{M} \sum_{n=1}^{N_k} \left(K_1(t_j^k, t_n^m)\omega_j^k + K_2(t_j^k, t_n^m)\overline{\omega_j^k} \right) = h_j^k \tag{24}$$

where $h_j^k = h(t_j^k)$ and the kernels K_1, K_2 are given by

$$K_1(t_j^k, t_n^m) = \frac{w_n^m}{\pi} \operatorname{Im}\left(\frac{d_n^m}{t_n^m - t_j^k}\right) + K_1^s(t_j^k, t_n^m) \tag{25}$$

$$K_2(t_j^k, t_n^m) = \frac{w_n^m}{\pi} \frac{\operatorname{Im}((t_n^m - t_j^k)\overline{d_n^m})}{\overline{(t_n^m - t_j^k)}^2} + K_2^s(t_j^k, t_n^m) \tag{26}$$

$$K_1^s(t_j^k, t_n^m) = \delta_m w_n^m \left(\frac{i\overline{d_n^m}}{\overline{t_j^k - z_m}} + 2\log|t_j^k - z_m| \right) \tag{27}$$

$$K_2^s(t_j^k, t_n^m) = \delta_m w_n^m \frac{t_j^k - z_m - i d_n^m}{\overline{t_j^k - z_m}} \tag{28}$$

where $\delta_m = 1$ excepts for $\delta_0 = 0$.

In the limiting case of $t_j^k = t_n^m$, the values of K_1, K_2 are:

$$K_1(t_j^k, t_j^k) = \frac{w_j^k \kappa_j^k |d_j^k|}{2\pi} + K_1^s(t_j^k, t_j^k) \tag{29}$$

$$K_2(t_j^k, t_j^k) = -\frac{w_j^k \kappa_j^k (d_j^k)^2}{2\pi |d_j^k|} + K_2^s(t_j^k, t_j^k) \tag{30}$$

where κ_j^k is the signed curvature at the point t_j^k.

By separating the real and imaginary parts of the Nyström discretizetion (24), we can get a $2N \times 2N$ matrix equation:

$$\begin{pmatrix} I + \operatorname{Re}(K_1 + K_2) & \operatorname{Im}(-K_1 + K_2) \\ \operatorname{Im}(K_1 + K_2) & I + \operatorname{Re}(K_1 - K_2) \end{pmatrix} \begin{pmatrix} \operatorname{Re}\omega \\ \operatorname{Im}\omega \end{pmatrix} = \begin{pmatrix} \operatorname{Re} h \\ \operatorname{Im} h \end{pmatrix} \tag{31}$$

This equation is solved iteratively by the GMRES [12]. For each GMRES iteration, evaluating the left hand side of (31) is done by a biharmonic fast multipole method (FMM) provided by the Flatiron Institute [4], which reduce the time complexity of each GMRES iteration from $O(N^2)$ to $O(N)$, and the overall space complexity from $O(N^2)$ to $O(N)$.

The matrix equation (31) has rank-1 deficiency, due to the zero-net-flux condition $\operatorname{Re}\int_\Gamma \overline{h(t)}dt = 0$ of Stokes equation. This rank-1 deficiency can cause GMRES to converge slowly. By adding a double layer term into (31) would fill up the nullspace of this BIE and avoid GMRES stagnating [15].

Once ω is solved, (9), (10), (12), and (14), can be applied to evaluate the velocity, pressure, and vorticity inside the domain. However, near the boundary, these evaluation involves nearly singular integrals. Thus, we have adopted the methods from [14, 7] for accurate evaluation of these physics quantities near the boundary.

[‡]The source code is available in the author's GitHub repository: stokes2d

3.2 Discretization and Smoothness of the Boundary

The boundary curves is discretized into a set of Gauss-Legendre panels, with certain heuristics applied to ensure that each panel resolves the curve accurately enough. Moreover, if two non-neighboring panels are very close to each other, the evaluation of left hand side of (31) might contain nearly singular integrals. Hence, such panels are further refined. These discretization strategies are nothing new from the detailed description of an adaptive refinement discretization scheme in [14].

The key to spectral convergence of GMRES is to have smooth boundary. For piecewise smooth boundary, a graded meshes can also be used to resolve corner singularity [14]. Here in this paper, we have used only smooth boundary curves, and how we have done it is explained as follows.

At each of the inlets and outlets, there are two right angle corners. These two right angles are avoided by adding superficial cap at the inlet and outlet, and putting the Poiseuille boundary conditions on the superficial cap instead. Figure 4a demonstrates an example, where the orange line demonstrate the original cornered geometry with Poiseuille boundary conditions, and the blue dashed-line denotes the superficial caps, with the same Poiseuille boundary condition denoted by the dark-blue color. The standard pieces are still connected along the orange straight line, in which case the blue caps are still in middle of a long straight channel. Therefore, the *return to Poiseuille* hypothesis still holds at the blue caps and it is numerically stable to transfer the Poiseuille velocity profile from the orange lines to the blue caps. These caps are smooth curves constructed as in Appendix B. of [1].

Other corners of the geometry are smoothed as in Figure 4b. This is achieved by a convolution the coordinates of the corner with a smooth bump function [3].

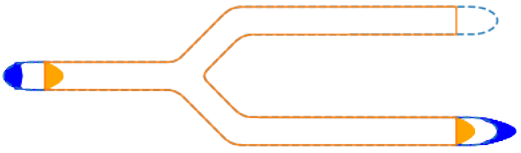

(a) Superficial Caps on 3 inlets/outlets of a Y-shaped standard piece

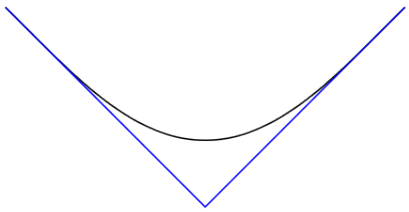

(b) A Smoothed Corner

Figure 4: Smoothed Geometry

4 Numerical Results and Discussion

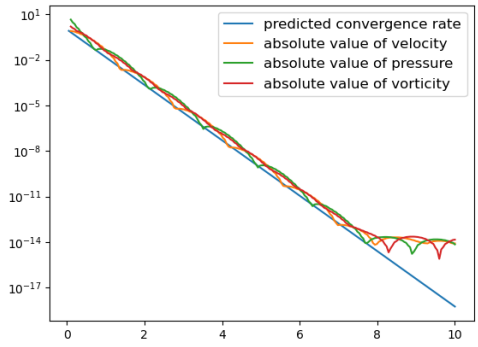

(a) Numerical convergence rate of return to Poiseuille flow in a straight channel

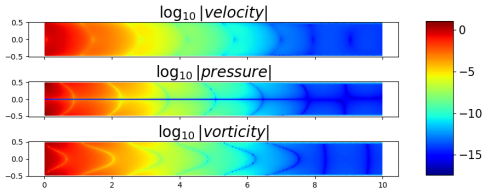

(b) $\log_{10}$ of the magnitude of the $(u, v), p, \zeta$ within the straight channel

Figure 5: Numerical exponential rate for return to Poiseuille flow. (a) The semilogy of magnitude of velocity, pressure, and vorticity along each vertical cross section along the channel. (b) The color plot of the magnitude of velocity, pressure, and vorticity in $\log_{10}$ scale in the straight channel.

4.1 Numerical Evidence of Return to Poiseuille

The numerical evidence for return to Poiseuille phenomenon is demonstrated on a straight channel of width 1 and length 10 as in Figure 5. On the left boundary, a smooth velocity profile is imposed. This velocity profile is an arbitrarily picked smooth function that satisfies the requirement of equation (18). On the rest of the curve, non-slippery condition is imposed.

Figure 5a shows that the rate of returning to the zero flow is agreed with the predicted rate from Section 2.2 up to 14th digits of accuracy. Figure 5b is a color plot where the color indicates the $\log_{10}$ of absolute value of the velocity, pressure, and vorticity.

4.2 A More Complicated Example

Figure 1 is an example of 22 pieces of 7 different kinds of standard pieces. Each of the standard pieces are solved

with 12 digits of accuracy, and are compared with a solution on the global geometry with 10 digits of accuracy.

No major numerical error can be observed near the interface of two standard pieces. This could mean that the *return to Poiseuille* is indeed good numerical hypothesis.

5 Conclusions

We have presented an usage of the *return to Poiseuille* phenomenon that turns the problem of solving Stokes flow on a channel geometry generated by several standard pieces into solving for weights (fluxes) on edges of a directed graph. It provides a way to instantly get high order accurate solutions for the special geometries considered in this paper.

One nature extension of this work is to make a 3D version, where more interesting standard pieces can be included. The major weakness of this work is that the current scheme relies heavily on the return to Poiseuille hypothesis, therefore it is cannot include particles in the flow, which is crucial for many applications. In this regard, a more useful extension of this work is to be able to add particles in the fluid simulations. It is possible to extend the interface idea to not only interface pre-solved Poiseuille flows, but also a larger class of pre-solved characteristic flows. And the influence of particles can be coupled with fast direct solvers. In this way, it might be possible to achieve fast and accurate simulations of Stokes flow with particles in it.

Acknowledgements

We thank Manas Rachh and Charles Peskin for many useful discussions pretaining to this work. We thank Manas Rachh and Libin Lu for providing support for the Flatiron Institute's FMM2D library [4].

References

[1] Joar Bagge and Anna-Karin Tornberg. Highly accurate special quadrature methods for Stokesian particle suspensions in confined geometries. 93(7):2175–2224.

[2] Horgan Co. Recent developments concerning Saint-Venant's principle,". In *In Advances in Applied Mechanics, TY Wu and JW Hutchinson (Eds), Vol 23,*, pages 179–269. Academic Press,.

[3] Charles L. Epstein and Michael O'Neil. Smoothed corners and scattered waves.

[4] Zydrunas Gimbutas, Leslie Greengard, Mike O'Neil, Manas Rachh, and Vladimir Rokhlin. Fmm2d.

[5] Leslie Greengard, Mary Catherine Kropinski, and Anita Mayo. Integral Equation Methods for Stokes Flow and Isotropic Elasticity in the Plane. 125(2):403–414.

[6] R. D. Gregory. The traction boundary value problem for the elastostatic semi-infinite strip; existence of solution, and completeness of the Papkovich-Fadle eigenfunctions. 10(3):295–327.

[7] Johan Helsing and Rikard Ojala. On the evaluation of layer potentials close to their sources. 227(5):2899–2921.

[8] C.O. Horgan. Decay Estimates for the Biharmonic Equation with Applications to Saint-Venant Principles in Plane Elasticity and Stokes Flows. 47(1):147–157.

[9] O. A. Ladyzhenskaya, Richard A. Silverman, Jacob T. Schwartz, and Jacques E. Romain. *The Mathematical Theory of Viscous Incompressible Flow*. 17(2):57–58.

[10] Nikolaj I. Muschelišvili and Nikolaj I. Muschelišvili. *Singular Integral Equations: Boundary Problems of Function Theory and Their Application to Mathematical Physics*. Wolters-Noordhoff Publishing, softcover reprint of the original 1st ed. 1958 edition.

[11] N. I. Muskhelishvili. *Some Basic Problems of the Mathematical Theory of Elasticity*. Springer Netherlands.

[12] Youcef Saad and Martin H. Schultz. GMRES: A Generalized Minimal Residual Algorithm for Solving Nonsymmetric Linear Systems. 7(3):856–869.

[13] Lloyd N. Trefethen. *Approximation Theory and Approximation Practice, Extended Edition*. Society for Industrial and Applied Mathematics.

[14] Bowei Wu, Hai Zhu, Alex Barnett, and Shravan Veerapaneni. Solution of Stokes flow in complex nonsmooth 2D geometries via a linear-scaling high-order adaptive integral equation scheme. 410:109361.

[15] Yabin Zhang, Adrianna Gillman, and Shravan Veerapaneni. A fast direct solver for integral equations on locally refined boundary discretizations and its application to multiphase flow simulations. 48(5):63.